The metal–insulator transition in the strongly correlated layered compound Na_yCoO_2 induced by dilute Mn doping

2004 J. Phys.: Condens. Matter 16 4935

(http://iopscience.iop.org/0953-8984/16/28/013)

INSTITUTE OF PHYSICS PUBLISHING JOURNAL OF PHYSICS: CONDENSED MATTER

J. Phys.: Condens. Matter **16** (2004) 4935–4940 PII: S0953-8984(04)77314-2

The metal–insulator transition in the strongly correlated layered compound $Na_\gamma CoO_2$ induced by dilute Mn doping

W Y Zhang[1], H C Yu[2], Y G Zhao[1,3], X P Zhang[1], Y G Shi[2], Z H Cheng[2] and J Q Li[2]

[1] Department of Physics, Tsinghua University, Beijing 100084, People's Republic of China
[2] Institute of Physics, Chinese Academy of Sciences, Beijing 100080, People's Republic of China

E-mail: ygzhao@tsinghua.edu.cn

Received 4 March 2004
Published 2 July 2004
Online at stacks.iop.org/JPhysCM/16/4935
doi:10.1088/0953-8984/16/28/013

Abstract

Structure, transport and magnetic properties have been investigated for the layered materials $Na_\gamma Co_{1-x}Mn_xO_2$ ($0 \leqslant x \leqslant 0.5$). With increase of the Mn concentration, the in-plane lattice parameter a decreases while the lattice parameter c increases. 3% Mn doping can result in a metal–insulator transition. The temperature dependence of the magnetization of the samples obeys the Curie–Weiss law and the effective moment of the magnetic ions increases with doping. Electron energy-loss spectroscopy measurement shows that the Co valence is about 3.3 and remains unchanged upon doping. However, the valence of Mn increases rapidly with doping and reaches 3.7 ± 0.1 for the sample with $x = 0.5$. The results are discussed in terms of the disorder effect induced by doping of magnetic ions. This work demonstrates that the structure, transport and magnetic properties of $Na_\gamma CoO_2$ are very sensitive to doping with magnetic ions.

1. Introduction

The layered compound $Na_\gamma CoO_2$ has attracted considerable attention due to its unique structure and physical properties, e.g., the large room temperature Seebeck coefficient 100 μV K^{-1} which is nearly ten times higher than those of typical metals [1–3], and the existence of superconductivity in the water-intercalated $Na_\gamma CoO_2$ compound, which is a breakthrough in the search for new layered transition metal oxide superconductors [4, 5]. The layered compound $Na_\gamma CoO_2$ has a two-dimensional (2D) crystal structure where Na ions and CoO_2 blocks are

[3] Author to whom any correspondence should be addressed.

alternately stacked along the c axis. Each Co ion is surrounded by slightly distorted oxygen octahedra and the Co ions form a 2D triangular lattice, which may be a realization of Anderson's original triangular lattice RVB system [6]. Charge carrier transport is thought to be restricted mainly to these CoO_2 planes, as in the case of the CuO_2 planes for the high T_c cuprates; thus the physical properties are expected to be highly 2D. For example, the resistivity of single-crystal $Na_\gamma CoO_2$ shows anisotropy both in magnitude and temperature dependence [1]. However, the 2D triangular lattice of Co ions in $Na_\gamma CoO_2$ is different from the 2D square lattice of cuprates and the effective hopping of 3d electrons between Co ions is reduced since the Co–O–Co bond angle is about 98.5° instead of 180° in cuprates [7, 8].

Evidence is accumulating to show that the compound $Na_\gamma CoO_2$ is a strongly correlated system [9–12]. In this kind of system, spin–charge–orbital interactions are usually in a subtle balance and dramatic change of physical properties could be induced with a slight variation in, e.g., the carrier density or lattice distortion which is closely related to the composition of the compounds. A number of experimental results show that Na-site substitution has strong influences on the physical properties of the compounds $Na_\gamma CoO_2$ [13–15]. Up to now, to our knowledge, little work has been done on the effect of Co-site substitution with magnetic ions on the structure and physical properties of the compounds $Na_\gamma CoO_2$. Terasaki *et al* [16] studied $NaCo_{2-x}Cu_xO_4$, focusing on the thermopower. It was found that the solid solubility limit of Cu in $NaCo_{2-x}Cu_xO_4$ is very small ($x = 0.2$) and the samples remain metallic. Doping has been proved very effective for uncovering the nature of the cuprates [17] and manganites, so it is essential to use different ions to substitute for Co in order to get some important information on the nature of $Na_\gamma CoO_2$.

In this paper, the effects of the substitution of Mn for Co on structure, transport and magnetic properties of the layered compounds $Na_\gamma CoO_2$ have been investigated. It is found that the solid solubility of Mn in $Na_\gamma CoO_2$ is very large, at least larger than the maximum doping ($x = 0.5$) in the present work. EELS measurements demonstrate that the valence states of manganese change clearly with increase of the doping level. A small amount of Mn substitution could induce a metal–insulator transition in $Na_\gamma CoO_2$. The effect of Mn doping was attributed to the electronic and magnetic disturbance due to that Mn doping.

2. Experimental details

Polycrystalline samples with nominal compositions $NaCo_{1-x}Mn_xO_2$ ($x = 0, 0.03, 0.05, 0.07, 0.1, 0.2, 0.3, 0.4, 0.5$) were prepared by solid-state reaction. Stoichiometric amounts of Na_2CO_3, Co_3O_4 and MnO_2 were mixed and sintered at 800–860 °C for 14 h in air. The product was finely ground, pressed into pellets and sintered at 800–900 °C for 10 h in air. Since Na tends to evaporate during calcinations [2], the undoped sample with the starting composition of $NaCoO_2$ is expected to change to about $Na_\gamma CoO_2$ with $0.70 < \gamma < 0.75$.

An x-ray diffraction study was performed using a Rigaku D/max-RB x-ray diffractometer with Cu Kα radiation as the x-ray source in the θ–2θ scan mode. The electrical resistivity $\rho(T)$ was measured using the four-probe method within the temperature range of 5–300 K. Indium was used for the electrical contact. The dc magnetization was measured using a superconducting quantum interference device (SQUID) magnetometer within the temperature range of 5–300 K in a 500 Oe magnetic field.

The TEM investigations were performed on a Tecnai F20 TEM (200 kV) equipped with a post-column Gatan imaging filter. The energy resolution in the EELS spectra is 0.7 eV under normal operation conditions. In order to minimize the radiation damage under electron beam exposure the samples were cooled below 200 K during our TEM observations.

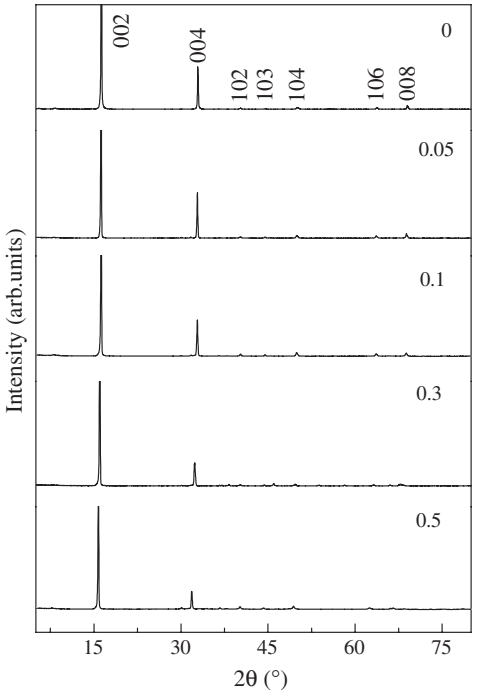

Figure 1. X-ray diffraction patterns of $Na_\gamma Co_{1-x}Mn_xO_2$ with different doping concentrations.

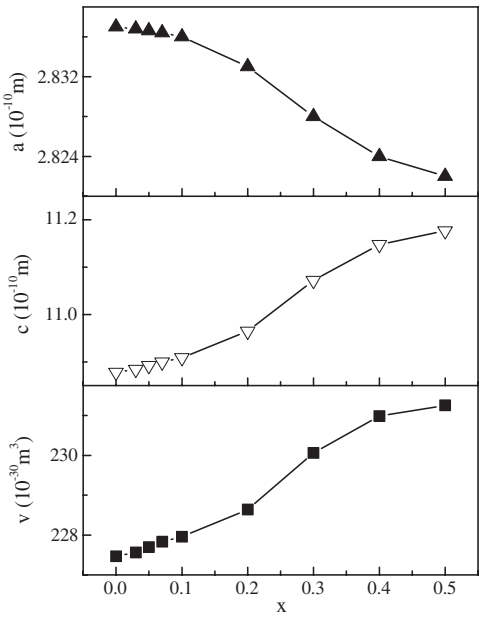

Figure 2. Variations of the lattice parameters a, c and unit cell volume with Mn content x.

3. Results and discussion

Figure 1 shows the x-ray diffraction patterns of the samples $Na_\gamma Co_{1-x}Mn_xO_2$. The Rietveld analysis reveals a hexagonal layered structure with space group of $P6_3/mmc$ and $a = 2.837$ Å, $c = 10.878$ Å for the sample with $x = 0$. The values of the lattice constant a and c determined here are in good agreement with the standard values of $a = 2.833$ Å and $c = 10.88$ Å obtained by Fouassier *et al* [15], suggesting that the sintered samples are γ phases of $Na_{0.70}CoO_2$. With x increasing, no additional peak appears, which shows that Mn is completely substituted for Co. It seems that the degree of solid solution with Mn can be further improved. Figure 2 shows the lattice constants a, c and unit cell volume of $Na_\gamma Co_{1-x}Mn_xO_2$ with respect to the concentration of Mn doping. With increase of the doping amount, the lattice parameter a decreases and the lattice parameter c increases. As a result, the unit cell volume of the samples increases with Mn doping. The variations of the lattice parameters a, c and unit cell volume can be understood by considering the valences of Co and Mn obtained from EELS as shown later.

EELS, a powerful technique for material characterization at nanometre spatial resolution, has been widely used in chemical microanalysis [18]. In order to obtain information on the valence states for both Co and Mn in the materials $Na_\gamma Co_{1-x}Mn_xO_2$, we have typically performed EELS analyses on $x = 0.1$ and 0.5 samples. Figure 3(A) shows the EELS spectra of the materials $Na_\gamma Co_{0.9}Mn_{0.1}O_2$ and $Na_\gamma Co_{0.5}Mn_{0.5}O_2$ taken from an area about 100 nm in diameter. In these spectra, the typical peaks, i.e. the collective plasmon peaks as well as core edges for Co, Mn and O elements, are displayed.

For transition metals with unoccupied 3d states, the transition of an electron from a 2p state to 3d levels leads to the formation of white lines. The L_3 and L_2 lines are for the transitions

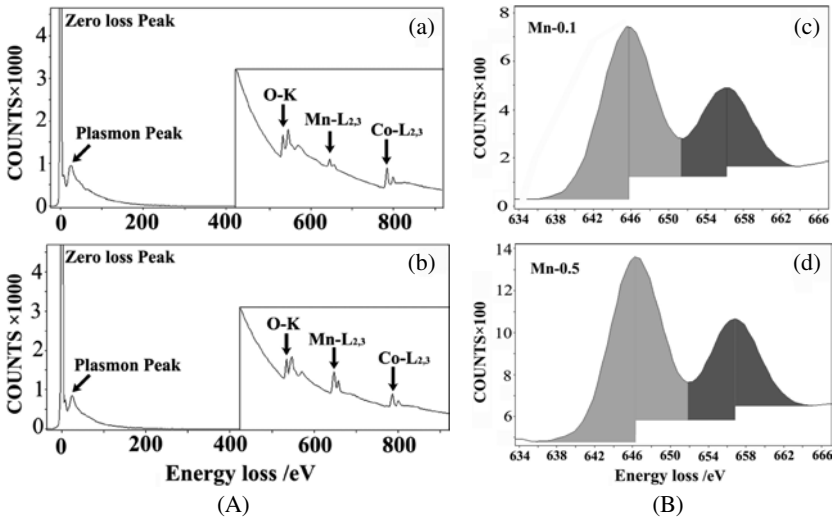

Figure 3. (A) EELS spectra of $Na_\gamma Co_{0.9}Mn_{0.1}O_2$ (a) and $Na_\gamma Co_{0.5}Mn_{0.5}O_2$ (b). (B) Typical spectra for the Mn L_2 and L_3 peaks obtained from $x = 0.1$ (c) and 0.5 (d) samples, respectively. The shaded area below each peak is used for intensity calculations. The left peak is L_3, while the right peak is L_2.

from $2p_{3/2}$ to $3d_{3/2}3d_{5/2}$ and from $2p_{1/2}$ to $3d_{3/2}$, respectively. Their intensities are related to the unoccupied states in the 3d bands. For the materials $Na_\gamma Co_{1-x}Mn_xO_2$, we have made a series of measurements in association with quantitative analyses by the method reported by Wang *et al* [18].

Our first measurement is performed on Co peaks in the spectra, the ratio of L_3/L_2 in general is around 2.4 and no evident change occurs along with increase of the Mn content. These data could yield a Co valence of about 3.3–3.4 for the samples with $x = 0.1$ and 0.5. This valence state is fundamentally in agreement with that obtained for the parent sample $NaCoO_2$ [19].

In contrast to the data obtained for the Co element, a remarkable change in the Mn peaks with the Mn content has been observed in our experiments. Figure 3(B) shows typical spectra for the Mn L_2 and L_3 peaks obtained from $x = 0.1$ and 0.5; in both spectra we schematically illustrate the extraction of the intensities for the white lines of the Mn element. The measurements for the sample with $x = 0.1$ indicate that the L_3/L_2 ratio is about 2.2, which could yield an average Mn valence of about 3.1–3.3 in this material [18]. The analyses of the sample with $x = 0.5$ give rise to an L_3/L_2 ratio of around 2.05; moreover, these data could change slightly from one crystalline grain to another. Our systematical analyses conclude that the Mn valence state ranges from 3.6 to 3.8 for the sample with $x = 0.5$.

In accordance with the EELS measurement, the Co^{3+}/Co^{4+} ratio is generally not equal to the Mn^{3+}/Mn^{4+} ratio in such materials; instead the Mn^{3+}/Mn^{4+} ratio changes much more quickly than the Co^{3+}/Co^{4+} ratio. Therefore Mn^{4+} ions not only substitute for Co^{4+}, but also substitute for some Co^{3+} ions and keep the Co^{3+}/Co^{4+} ratio constant. In order to keep the charge balance, either the content of Na decreases or the oxygen content increases. On the basis of the valences of Mn and Co, the variations of the lattice parameters a, c and unit cell volume of $Na_\gamma Co_{1-x}Mn_xO_2$ can be understood by considering the ion radii of Co^{3+} (0.685 Å), Co^{4+} (0.67 Å), Mn^{3+} (0.72 Å) and Mn^{4+} (0.67 Å) [20]. The ion radius of Mn^{3+} is larger than those of Co^{3+}, Co^{4+} and Mn^{4+}. So Mn doping is expected to increase the unit cell volume and the slope

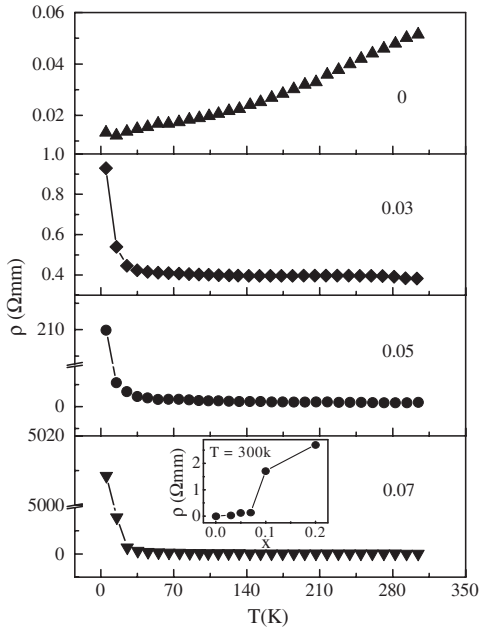

Figure 4. The variation of resistivity with temperature for $Na_\gamma Co_{1-x}Mn_xO_2$. The inset shows the dependence of the room temperature resistivity on the Mn content x.

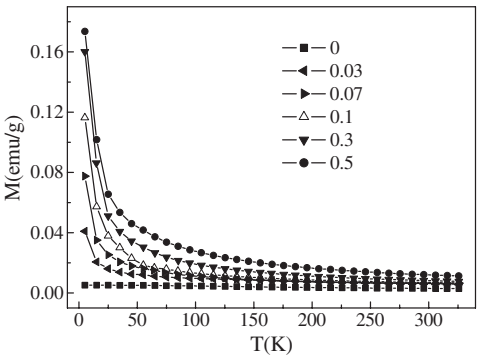

Figure 5. The temperature dependence of the magnetization for the samples $Na_\gamma Co_{1-x}Mn_xO_2$.

will decrease with Mn doping due to the decrease of the Mn^{3+}/Mn^{4+} ratio, consistent with the unit cell volume variation shown in figure 2. Since Mn^{3+} is a Jahn–Teller ion, distortion with in-plane contraction and out-of-plane (c axis) elongation may occur, leading to a decrease of the in-plane lattice parameter a.

The variation of resistivity with temperature for $Na_\gamma Co_{1-x}Mn_xO_2$ is shown in figure 4. It can be clearly seen that a low level doping with 3% Mn replacing Co leads to a metal–insulator transition, in contrast to the case for $NaCo_{1-x}Cu_xO_2$ [16]. Since the lattice parameter c increases with Mn doping, the coupling between the CoO_2 layers decreases and the 2D nature of the CoO_2 becomes more prominent with Mn doping. Generally, it is known that the physical properties of low dimensional systems are very sensitive to disorder; the metal–insulator transition in $Na_\gamma Co_{1-x}Mn_xO_2$ is therefore expected to be related to the Anderson localization induced by the disorder effect. Because $NaCo_{1-x}Cu_xO_2$ remains metallic up to $x = 0.1$, which is the solid solubility limit for Cu in $NaCoO_2$ [16], the contribution of magnetic disturbance to the CoO_2 layers due to Mn doping may play an important role. It should be pointed out that the metal–insulator transition occurs at a very low doping level, so its origin is expected to be related to the Mn doping effect rather than the possible minor change of oxygen content. The inset of figure 4 presents the dependence of the room temperature resistivity of $Na_\gamma Co_{1-x}Mn_xO_2$ on the Mn content. The resistivity increases gradually with x and an abrupt increase occurs at around 0.07. It has been shown that the distance between the Co is very important for determining the electrical properties and a critical distance R_c can be used to judge whether $NaMO_2$ (M = Cr, Mn, Fe, Co, Ni) is a metal or an insulator [21, 22]. The same feature may be also useful for the doped systems. The transport mechanism of doped $Na_\gamma CoO_2$ needs further study.

Figure 5 shows the result of dc magnetization for the samples $Na_\gamma Co_{1-x}Mn_xO_2$. All the samples exhibit Curie–Weiss behaviour, indicating the existence of a localized moment.

Using the Curie–Weiss law $\chi = \chi_0 + C/(T - \theta)$ to fit the experimental data, where θ is the paramagnetic Curie–Weiss temperature, χ_0 is a sum of temperature-independent terms and $C = N\mu_{\text{eff}}^2/3k_{\text{B}}$ (μ_{eff} is the effective moment of magnetic ions, k_{B} is the Boltzmann constant and N is the number of magnetic ions per unit volume), we can deduce that the effective magnetic moment of the system increases with Mn doping. This can be attributed to the large magnetic moments of Mn^{3+} and Mn^{4+}, and the replacement of nonmagnetic Co^{3+} ions by Mn^{3+} and Mn^{4+} ions.

4. Conclusions

Single-phase layered samples of $Na_\gamma Co_{1-x}Mn_xO_2$ were prepared by solid-state reaction. Upon Mn doping, the lattice parameter a decreases and the lattice parameter c increases rapidly, which leads to expansion of the unit cell volume. $Na_\gamma Co_{1-x}Mn_xO_2$ is very sensitive to Mn doping; as a result, substitution of 3% Mn for Co results in a metal–insulator transition. The temperature dependence of the magnetic moment for the samples $Na_\gamma Co_{1-x}Mn_xO_2$ obeys the Curie–Weiss law and the effective magnetic moment increases along with the Mn doping. The results can be explained by considering the valence states of Co and Mn, the variation of the coupling between the CoO_2 layers and the disorder induced by Mn doping.

Acknowledgments

This work was supported by NSFC (project No 50272031), the Excellent Young Teacher Programme of MOE, PRC, National 973 project (No 2002CB613505) and the Specialized Research Fund for the Doctoral Programme of Higher Education (No 20030003088).

References

[1] Terasaki I, Sasago Y and Uchinokura K 1997 *Phys. Rev.* B **56** R12685
[2] Koshibae W, Tsutsui K and Maekawa S 2000 *Phys. Rev.* B **62** 6869
[3] Motohashi T, Naujalis E, Ueda R, Isawa K, Karppinen M and Yamauchi H 2001 *Appl. Phys. Lett.* **79** 1480
[4] Takada K, Sakurai H, Takayama-Muromachi E, Izumi F, Dilanian R A and Sasaki T 2003 *Nature* **6** 53
[5] Schaak R E, Klimczuk T, Foo M L and Cava R J 2003 *Nature* **424** 527
[6] Anderson P W 1973 *Mater. Res. Bull.* **8** 153
Anderson P W 1987 *Science* **235** 1996
[7] Jansen Von M and Hoppe R 1974 *Z. Anorg. Allg. Chem.* **408** 104
[8] Singh D J 2000 *Phys. Rev.* B **61** 13397
[9] Ando Y, Miyamoto N, Segawa K, Kawata T and Terasaki I 1999 *Phys. Rev.* B **60** 10580
[10] Ray R, Ghoshray A, Ghoshray K and Nakamura S 1999 *Phys. Rev.* B **59** 9454
[11] Wang Y, Rogado N S, Cava R J and Ong N P 2003 *Nature* **423** 425
Wang Y, Rogado N S, Cava R J and Ong N P 2003 *Preprint* cond-mat/0305455
[12] Motohashi T, Ueda R, Naujalis E, Tojo T, Terasaki I, Atake T, Karppinen M and Yamauchi H 2003 *Phys. Rev.* B **67** 064406
[13] Kawata T, Iguchi Y, Itoh T, Takahata K and Terasaki I 1999 *Phys. Rev.* B **60** 10584
[14] Rivadulla F, Zhou J S and Goodenough J B 2003 *Phys. Rev.* B **68** 075108
[15] Fouassier C, Matejka G, Reau J-M and Hagenmuller P 1973 *J. Solid State Chem.* **6** 532
[16] Terasaki I, Tsukada I and Iguchi Y 2002 *Phys. Rev.* B **65** 195106
[17] Xiao G, Cieplak M Z, Xiao J Q and Chen C L 1990 *Phys. Rev.* B **42** 8752
Tarascon J M, Barboux P, Miceli P F, Greene L H, Hull G W, Eibschutz M and Sunshine S A 1988 *Phys. Rev.* B **37** 7458
[18] Wang Z L, Yin J S and Jiang Y D 2000 *Micron* **31** 571
[19] Shi Y G, Li J Q, Yu H C, Zhou Y Q, Zhang H R and Dong C 2004 *Supercond. Sci. Technol.* **17** 42–6
[20] Shannon R D 1976 *Acta Crystallogr.* A **32** 751
[21] Molenda J 1986 *Solid State Ion.* **21** 263
[22] Goodenough J B 1971 *Progress in Solid State Chemistry* vol 5, ed H Reiss (Oxford: Pergamon)